Spin-liquid signatures in geometrically frustrated layered kagome compounds $YBaCo_{4-x}Fe_xO_{7+\delta}$

Shainee Hazra,[1] A. K. Bera,[2] Swastika Chatterjee,[3] Anushree Roy,[1,*] and S. M. Yusuf[2,4,†]

[1]*Department of Physics, Indian Institute of Technology Kharagpur 721302, India*
[2]*Solid State Physics Division, Bhabha Atomic Research Centre, Mumbai 400085, India*
[3]*Department of Earth Sciences, Indian Institute of Science Education and Research, Kolkata 741246, India*
[4]*Homi Bhabha National Institute, Anushaktinagar, Mumbai 400094, India*

(Received 20 July 2020; revised 23 August 2021; accepted 6 October 2021; published 21 October 2021)

Experimental detection of spin dynamics of the quantum spin liquid phase, which occurs when the quantum fluctuations lead to fractionalized spin states, remains a challenge. In this paper, we illustrate spin-liquid signatures in the geometrically frustrated layered kagome system $YBaCo_{4-x}Fe_xO_{7+\delta}$ ($x = 0$ and $x = 0.6$) over a wide temperature range using micro-Raman spectroscopy. The thermal response of the gapped broad band over a high temperature range possibly marks a spin liquid phase in this system. We report the appearance of sharp spectral features in the high temperature regime with unusual thermal behavior for $YBaCo_{4-x}Fe_xO_{7+\delta}$ ($x = 0.6$). Besides, atypical oscillation of a phonon mode frequency with temperature suggests an unconventional electron-lattice coupling in the doped compound via a strong correlation between their lattice vibration and magnetic spin dynamics.

DOI: 10.1103/PhysRevB.104.144418

I. INTRODUCTION

In recent years, elusive elementary quasiparticle excitations in a certain class of materials have drawn special attention because of the rich physics which governs their characteristics. However, the experimental detection of these quasiparticles still remains a challenge as the manifestations of their probed features are weak; those are often obscured by the other signatures of the system. The electronic states of a group of strongly magnetic correlated systems exhibit gapped or gapless fractionalized electronic excitations and are believed to host these elementary quasiparticle excitations. The compounds with the quantum spin liquid (QSL) state, where a conventional magnetic ordering is absent due to the quantum fluctuations, are one of them [1–6]. Thus, the spin-liquid phase endows a paradigm beyond the Landau theory of phase transition. Topological ordering is one of the key characteristics of the symmetry-breaking gapped QSL phase, which exhibits long-ranged many-body entanglement and fractionalized excitations beyond one dimension. The microscopic spin-spin correlation in these systems has been probed by rigorous theories using the model Hamiltonian based on Heisenberg [6], Kitaev [7], Heisenberg-Kitaev [8], Shastry-Sutherland [9], Chern-Simons [10], and other interactions. Experimentally it has been demonstrated that irridate [11–13] and ruthenate [14,15] compounds exhibit the Kitaev-like interaction and show fractionalized excitations. The compound $SrCu_2(BO_3)_2$ shows a QSL ground state on the Shastry-Sutherland lattice [16,17]. Other canonical examples of QSL candidates include the $S = 1/2$ Heisenberg antiferromagnet on the kagome lattice of herbertsmithite $[ZnCu_3(OH)_6Cl_2]$ [6,18], and the triangular lattice of κ-$(BEDT\text{-}TTF)_2Cu_2(CN)_3$ [19] and $YbMgGaO_4$ [20].

Raman spectroscopy is one of the promising probes to detect elementary excitations in the QSL phase. In recent years, there has been significant progress in understanding the Raman response of the QSL antiferromagnets [21–24]. In this paper, we report a comprehensive micro-Raman spectroscopic study on a geometrically frustrated spin system $YBaCo_xFe_xO_{7+\delta}$ ($x = 0$ and 0.6) with an alternate layer of triangular and kagome lattice. The thermal response of the broad Raman peak over 40–110 meV possibly indicates the existence of a gapped QSL phase in these compounds. Furthermore, the appearance of additional sharp spectral features over a high temperature regime and their unusual thermal behavior are to be noted. We also report a strong electron-lattice coupling over the entire temperature range of measurements (80–300 K), in which the lattice vibration correlates with the spin fluctuation in an unusual manner.

II. METHODS

$YBaCo_{4-x}Fe_xO_{7+\delta}$ ($x = 0$, and 0.6) were synthesized using a solid-state reaction method [25,26]. Micro-Raman spectroscopic measurements of the compounds were carried out using a single monochromator (model iHR550, Make JY, Horiba, France) Raman spectrometer and a Peltier cooled charge-coupled device (CCD) (1024×256 pixels) detector. The spectrometer is equipped with an optical microscope (model BX41, Make Olympus, Japan). A 532 nm laser source was used as the excitation wavelength. The measurements were taken in backscattering geometry using a 50× objective lens (NA = 0.5). We tested the effect of laser power on the samples. Spectra of the compounds were recorded for incident

*anushree@phy.iitkgp.ac.in
†Corresponding author: smyusuf@barc.gov.in

powers of 9.4, 6.4, 3.6, 2.3, and 1.0 mW. The Raman modes suffered a redshift between 2.3 and 9.4 mW. However, no significant change in the Raman shift was observed for incident powers between 1.0 and 2.3 mW. Thus, all subsequent experiments were performed with a 1 mW power incident on the sample. The integration time for all measurements was kept fixed for 600 s for all the samples.

Temperature dependent Raman measurements over 80–300 K were carried out using a sample stage and a temperature controller along with a liquid nitrogen pump (THMS-600, Linkam, UK). We carried out three independent sets of measurements on both compounds under study. To rule out the effect of photoluminescence in the spectra, room temperature measurements were recorded using the triple monochromator Raman spectrometer (T64000, make JY, France) with 502- and 530-nm excitation lines of an Ar^+-Kr^+ ion laser.

The crystal structures of the present compounds $YBaCo_{1-x}Fe_xO_7$ ($x = 0$ and 0.6) were studied using neutron diffraction measurements and are available in [25,26]. Rietveld refinements of the neutron diffraction patterns of the compounds suggest that their crystal structure can be described either by the space group $P31c$ with trigonal symmetry or by $P6_3mc$ with hexagonal symmetry. The lattice parameters obtained from the Reitveld refinement of the diffraction patterns by these space groups are used as the initial input in our calculation. We performed first principles spin-polarized density functional theory (DFT) based calculations using the Vienna Ab-initio Simulation Package (VASP) [27–29] considering the generalized gradient approximation (GGA) [30]. For the exchange-correlation functional, we used the GGA as implemented in Perdew-Burke-Ernzerhof (PBE-GGA) [28] formulation. We adopted projector augmented wave (PAW) potentials, and the wave functions were expanded in a plane wave basis with the kinetic energy cutoff of 900 eV. Monkhorst-Pack k-mesh sampling of size $7\times7\times7$ was used for our calculation. To ensure the convergence of electronic energies during the self-consistent run and the calculation of Hellmann-Feynmann forces on atoms during structural optimization using conjugate gradient algorithm, a convergence criterion of 1×10^{-8} eV and 1×10^{-3} eV/Å, respectively, was followed. Gamma point phonon frequencies were obtained using density functional perturbation theory (DFPT) as implemented in the VASP code.

III. RESULTS AND DISCUSSION

The crystal structure of the studied compounds $YBaCo_{4-x}Fe_xO_{7+\delta}$($x = 0$ and 0.6) consists of an alternating stacking of distorted kagome and triangular layers of CoO_4 tetrahedra along the c axis [Fig. 1(a)] [25,26]. The Rietveld refined x-ray diffraction patterns with the space group $P31c$ of $YBaCo_xFe_xO_{7+\delta}$ ($x = 0$ and 0.6) are shown in Fig. 1(b). It has been shown earlier [25,26] that the crystal structure of the same compounds can be described either by the space group $P31c$ with trigonal symmetry or by $P6_3mc$ with hexagonal symmetry. The results obtained from a detailed analysis of the patterns are available in Refs. [25,26].

The compounds $YBaCo_{4-x}Fe_xO_{7+\delta}$ are regarded as mixed-spin [$S = 3/2$ for $Co^{2+}(3d^7)$, $S = 2$ for $Co^{3+}(3d^6)$, and

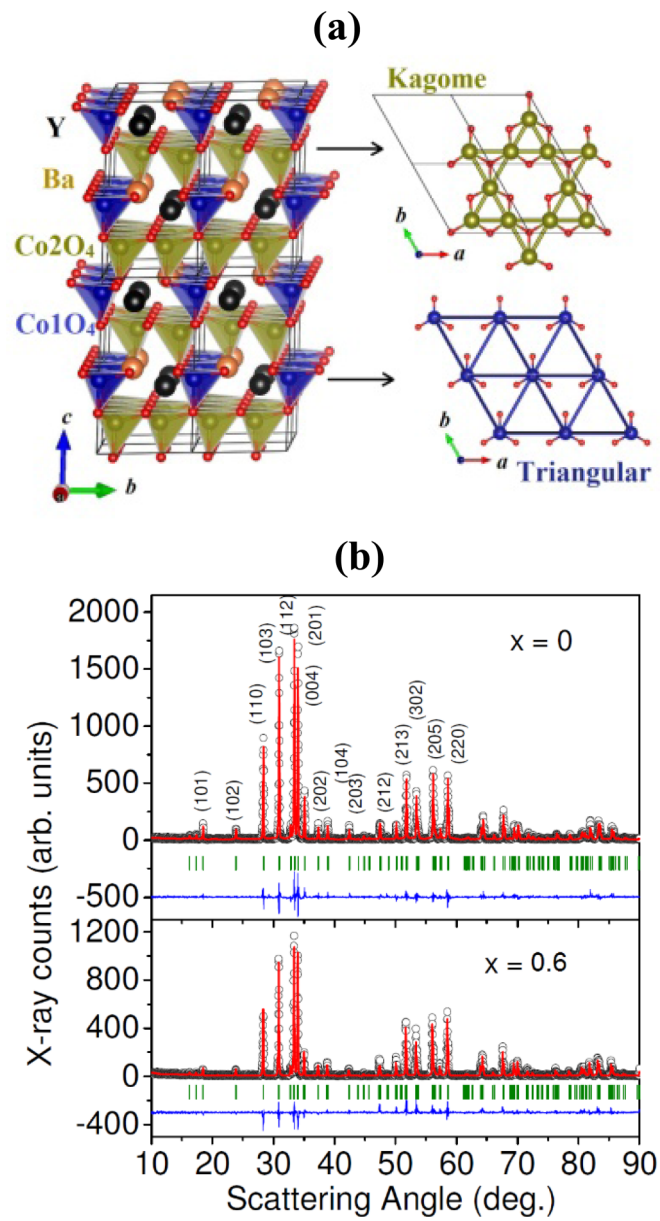

FIG. 1. (a) The layered crystal structure of $YBaCo_4O_7$. The atomic arrangements within the individual kagome and triangular lattice planes are shown. (b) The Rietveld refined x-ray diffraction patterns of compounds $YBaCo_{4-x}Fe_xO_{7+\delta}$ ($x = 0$ and 0.6) are measured at room temperature. The experimental and calculated patterns are shown by the open circles and solid red lines, respectively. The difference patterns are shown by the solid blue line at the bottom of each panel. The green bars correspond to the positions of the diffraction peaks for the phase $P31c$.

$S = 5/2$ for $Fe^{3+}(3d^5)$] Heisenberg antiferromagnetic (AFM) systems. The previous powder neutron diffraction studies confirmed short-range magnetic correlations in these systems below ~110 K down to 1.5 K [25,26,31–33]; however, they have a very high AFM Curie-Weiss temperature ($\theta_{CW} \sim$ –900 K for the $x = 0$ compound), revealing a strong geometrical spin frustration. Single crystal neutron diffraction measurements [34] further revealed quasi-one-dimensional magnetic correlations along the c axis and spin-liquid-like

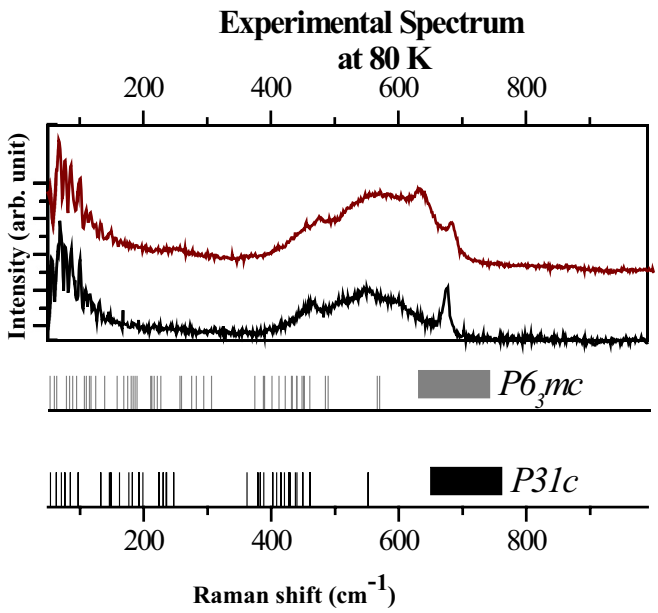

FIG. 2. Raman spectra of $YBaCo_4O_{7+\delta}$ (black) and $YBaCo_{3.6}Fe_{0.4}O_7$ (maroon) at 80 K over the spectral range 50–1000 cm^{-1}. Calculated Γ point phonon modes of $YBaCo_4O_7$ for the space group $P31c$ and $P6_3mc$ are shown by black and blue bars in the lower part of the figure.

correlations within the kagome layer (*ab* plane). Besides, the muon spin-relaxation investigations on $YBaCo_4O_{7+\delta}$ demonstrate a viscous spin liquid phase within the kagome sublattice [35]. With the increasing Fe concentration in $YBaCo_{4-x}Fe_xO_{7+\delta}$, an enhancement of the geometrical frustration, and, as a consequence, a decrease in the AFM short-range spin-spin correlations, and a sharp increase in the θ_{CW} value have been reported [26]. Further, the Fe^{3+} substitutions introduce spin disorders as well as bond/exchange disorders in the system [26].

The micro-Raman spectrum of $YBaCo_4O_{7+\delta}$, measured at 80 K, over the spectral window between 50 and 1000 cm^{-1}, is shown by the black solid line in Fig. 2(a). Other than several low wave-number sharp phonon peaks, we observe a broad band, centered at ∼580 cm^{-1} and width of ∼300 cm^{-1}, and a sharp peak at ∼695 cm^{-1} (assigned as peak $P1$). The observed sharp Raman modes suggest a well-ordered crystal lattice. The broad spectral feature is also evident in the Raman spectra reported earlier for $YBaCo_4O_{7+\delta}$ [36–38]. The high quality of our data allows us to unambiguously separate the broad peak from the sharp Raman modes. Our *ab initio* calculations, using the reported space groups (both hexagonal $P6_3mc$ and trigonal $P31c$) and the lattice parameters for $YBaCo_4O_{7+\delta}$ [25,26], reveal that there are a large number of phonon modes only below 500 cm^{-1}, some of which could be identified in the experimental Raman spectrum [Fig. 2(a)]. However, the broad band between 400 and 700 cm^{-1} and the sharp feature at $P1$ cannot be assigned to any of the calculated normal modes. It is unlikely that the broad band is the convolution of sharp features. Raman spectrum of $YBaCo_{3.6}Fe_{0.4}O_{7+\delta}$, measured at 80 K, is shown by the maroon solid line in Fig. 2(b). Along with all the above spectral features, an additional peak at 640 cm^{-1} appears in the doped compound.

Temperature dependent Raman spectra of the compounds over 80–300 K were recorded at a temperature interval of 5 K between 120 and 250 K, and at a temperature interval of 10 K between 250 and 300 K. A 2 K interval (with resolution 0.2 K) was chosen over the range between 80 and 120 K. Raman response χ'' is obtained upon the division of measured Raman intensity $I(\omega)$ by the thermal Bose factor, $\chi'' \propto I(\omega)/[1+n(\omega)]$, where $1+n(\omega) = 1/(1-e^{-\hbar\omega/k_BT})$. A few characteristic Raman responses of $YBaCo_{4-x}Fe_xO_{7+\delta}$ ($x = 0$ and 0.6) over 80–300 K are shown in Figs. 3(a) and 3(b), respectively. All spectra exhibit the presence of the broad band and the sharp peak $P1$. In addition, for $YBaCo_{3.4}Fe_{0.6}O_7$ multiple sharp spectral features over the broad band are observed between 230 and 270 K [see Fig. 3(c)].

First, we focus on the broad Raman response centered at ∼580 cm^{-1} (75 meV) with the onset at ∼320 cm^{-1} (∼40 meV). A broad spectral feature may appear due to the photoluminescence from a sample. Such possibility has been ruled out as there is no shift in the broad peak position for the measurements with laser excitation wavelengths 502 and 530 nm (see Fig. S1 in the Supplemental Material [39]). A convoluted phonon spectrum is expected to get resolved with the lowering of temperature. It is to be noted that the emergence of sharp spectral features is observed over the high temperature range between 230 and 270 K. Moreover, the thermal behavior of these sharp peaks is distinctly different from that of a phonon mode (to be discussed later in this paper). This discards the argument of whether the broad band is the convolution of many modes arising from phonon spectra in the compound. Moreover, the appearance of this broad peak up to room temperature negates its genesis to be a two-magnon peak. The broad band may also arise due to the interorbital transition. However, the energy scales of these types of transitions are generally of the order of a few eV [40,41] as compared to the peak energy of ∼75 meV in the present case.

Before we discuss the origin of the broad band in the Raman response plots, we refer to the structural and magnetic correlation in the present compounds ($YBaCo_{1-x}Fe_xO_7$ with $x = 0$ and 0.6), as obtained from neutron diffraction and Mössbauer spectroscopic measurements and reported elsewhere [25,26]. From the detailed analysis of the neutron diffraction patterns [26], the distortion in the kagome lattice, quantified by the difference between Co-Co distances of two unequal triangles in the kagome plane, is found to be significantly less in the doped compound. The distortion of the CoO_4 tetrahedron, quantified by estimating $\Delta = \frac{1}{4}\sum_i^4 \{(d_i - \langle d\rangle)/\langle d\rangle\}^2$, where d_i and $\langle d\rangle$ are i^{th} and average bond lengths of the tetrahedron, respectively, is also much less in $YBaCo_{3.6}Fe_{0.4}O_7$ than in the parent compound. The x-ray diffraction patterns (in Fig. 1) reveal that the presence of impurity phases is much less in the doped compound. It has been claimed that the decrease in the distortion of the kagome plane with Fe doping enhances the degree of spin frustration in the system. Furthermore, $YBaCo_xFe_{1-x}O_{7+\delta}$ did not exhibit any structural phase transition over the temperature range between 20 and 300 K [26]. Interestingly, while the magnetization plot revealed a strong anomaly below 80 K, the neutron diffraction data demonstrated an onset of magnetic ordering at a much higher temperature, ∼110 K [25]. It has been argued that a very short-range antiferromagnetic

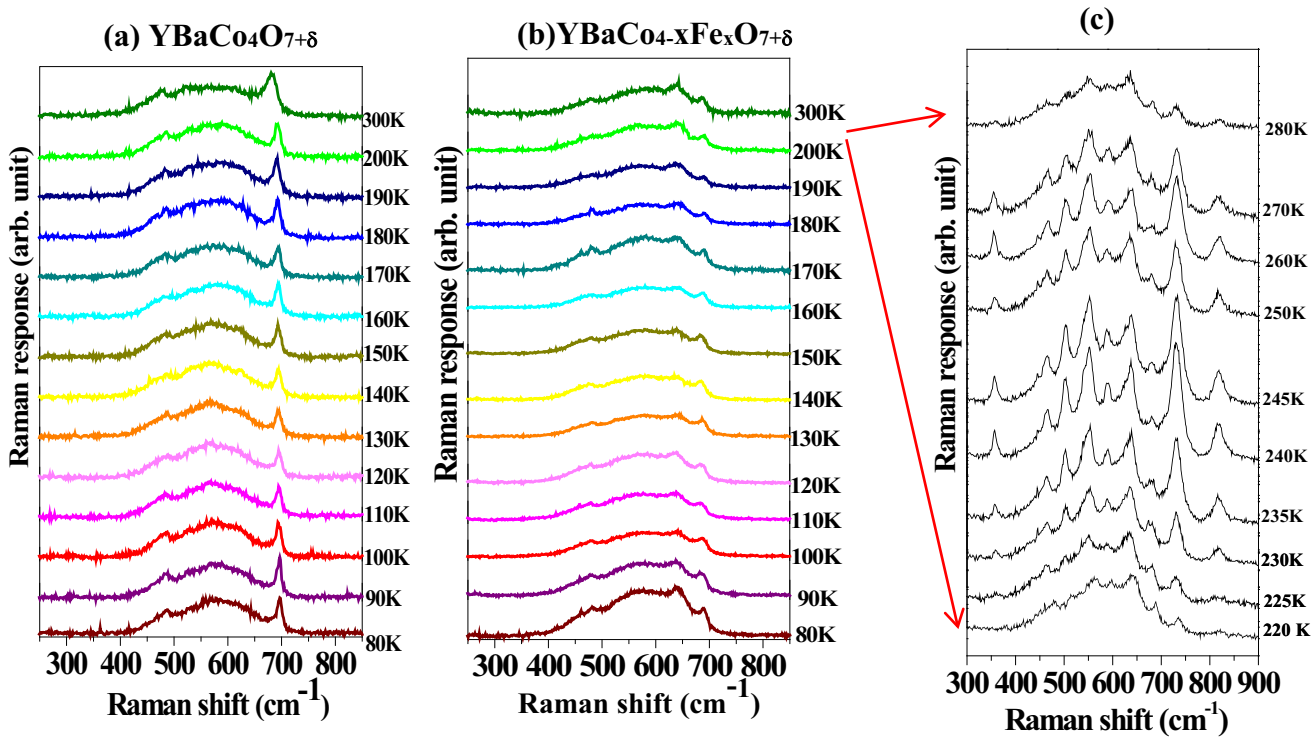

FIG. 3. Characteristic Raman response (χ'') of (a) $YBaCo_4O_{7+\delta}$ and (b) $YBaCo_{3.4}Fe_{0.6}O_{7+\delta}$ recorded between 80 and 300 K over the spectral range 250–850 cm^{-1}. (c) The same over the temperature range 220–280 K of the doped compound.

ordering exists in these compounds between 80 and 110 K [26]. Unusual temperature dependence of the lattice parameter and unit cell volume over this range of temperature is also reported. The frequency-independent behavior of the AC susceptibility plot and the linearity of the isotherm magnetization curves as a function of the magnetic field rule out the possibility of a spin-glass phase in these systems [26]. The very high Curie-Weiss temperature suggests that the magnetic state over 110–900 K is not in a true paramagnetic phase.

We believe that in the present study, the above discussed unconventional magnetic behavior is reflected in the Raman response of the broad band between 80 and 300 K. Raman response of the broad band between 80 and 100 K with a 2 K interval is shown in Fig. S2 of the Supplemental Material [39]. The integrated area under the broad band has been estimated (see Fig. S3 in Supplemental Material [39]). With increasing temperature from 80 K, a nearly linear decrease of the integral intensity of the broad peak is found up to ∼100 K for the $x = 0.6$ compound, whereas a constant behavior is observed for the parent compound (Fig. 4). It is interesting to note that the temperature range 80–100 K, over which a linear drop in Raman response is observed, falls in the temperature regime over which the neutron diffraction data indicated a short-range ordering in the system [25,26]. With further increasing temperature, the intensity of Raman response exhibits considerable modulation (see Fig. 4), indicating a complex interplay between thermal and spin fluctuations in these compounds. As mentioned above, the decrease in the distortion of the kagome plane with Fe doping enhances the degree of spin frustration in the system. This could be one of the reasons for the clear manifestation of unusual spin state in Raman response in $YBaCo_{3.6}Fe_{0.4}O_7$, which got masked by the lattice distortion in the parent compound. It is interesting to note that the broad mode survives till room temperature. For geometrically frustrated spin system $YBaCo_{4-x}Fe_xO_{7+\delta}$, having high

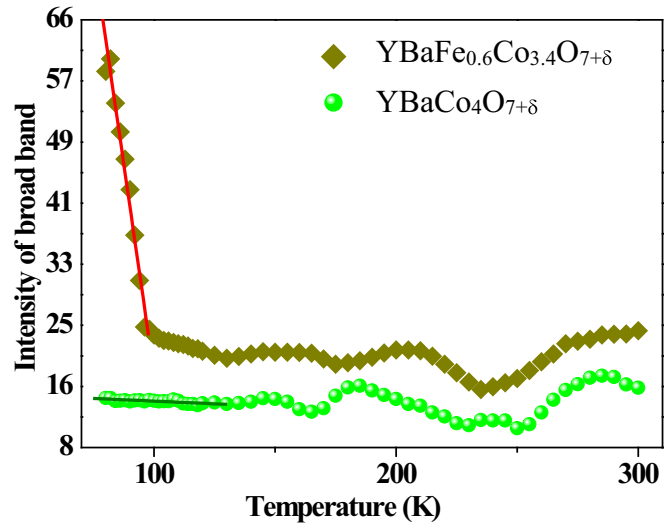

FIG. 4. The variation in the integral Raman response of the broad Raman band between 80 and 300 K for $YBaCo_4O_{7+\delta}$ (filled green circles) and $YBaCo_{3.4}Fe_{0.6}O_{7+\delta}$ (dark yellow diamonds). The linear fit to the data points in the low temperature regime is shown by solid lines. To estimate the error bar to the intensity of the broad band, first the sharp Raman peaks are removed manually from the spectra. The normalized difference between the integral intensity of the upper and lower envelope of the broad band at each temperature is taken as the error to intensity of the broad band. The estimated error bars of the data points are within the size of the symbols.

$\theta_{CW} > 900$ K, strong short-ranged spin-spin correlations much above the ordering temperature have been reported [32,34]. Unlike the magnon, the broad excitations of the spin-liquid state are less sensitive to the temperature and, therefore, are expected to persist up to high temperatures [10].

A similar broad continuum in the Raman spectra and its linear temperature dependence were reported for the $S = 1/2$ kagome Heisenberg AFM herbertsmithite $ZnCu_3(OH)_6Cl_2$, a well known quantum spin-liquid candidate [18]. The existence of a continuum is explained by considering two-spinon-two-antispinon operators in the Dirac spin-liquid ansatz. Moreover, the continuum in the neutron scattering spectra of $ZnCu_3(OH)_6Cl_2$ was interpreted in terms of fractionalized spin excitations of spinons [6,42,43]. By analogy to $ZnCu_3(OH)_6Cl_2$, the broad continuum in the Raman spectra and its temperature dependence yield the possibility of spin-liquid state in the studied compounds $YBaCo_{4-x}Fe_xO_{7+\delta}$. However, there are a few fundamental differences between our results from Raman spectroscopy and that for the spin-1/2 kagome compound $ZnCu_3(OH)_6Cl_2$, especially, a relatively large energy gap of ∼40 meV for the present compound and the fluctuation in the Raman intensity above 100 K (Fig. 4). The presence of crystal structural distortion in the kagome lattice can significantly change the underlying physics and subsequently the Raman spectrum, as reported for the spin-1/2 kagome systems vesignieite $BaCu_2V_2O_9(OH)_2$ and volborthite $Cu_3V_2O_7(OH)_2 \cdot 2H_2O$ [44]. With the increasing degree of lattice distortions, it is reported that the deconfined spin excitations get confined and behave like magnons [44]. The Raman spectrum for vesignieite includes more defined excitation modes than that of the herbertsmithite $ZnCu_3(OH)_6Cl_2$ with clear onset and cutoff energies. On the other hand, for the most distorted volborthite $Cu_3V_2O_7(OH)_2 \cdot 2H_2O$, the appearance of additional sharp Raman modes is reported at low temperatures [44]. The observed results from Raman measurements in the present study along with the reported neutron diffraction, magnetization plots, and Mossbauer spectroscopic measurements [25,26] indicate an unusual spin state in $YBaCo_{4-x}Fe_xO_{7+\delta}$.

It was intriguing to observe the sharp spectral features along with the broad band, shown in Fig. 3(c), over the temperature range 225–270 K. It is to be noted that the broad feature appeared again beyond 270 K. Figure 5(a) plots Raman response of $YBaCo_{3.6}Fe_{0.4}O_7$ at 245 K over the spectral range 330 cm^{-1} (40 meV)–930 cm^{-1} (110 meV). We deconvolute the spectrum with ten Lorentzian functions for the sharp features and one Gaussian function for the broad band, keeping peak positions, widths, and intensities of all sharp modes as free fitting parameters. The deconvoluted components are shown by solid black lines and marked as $X1$–$X10$. The peak position and the width of the Gaussian mode were fixed at 580 and 300 cm^{-1}. The net fitted spectrum is shown by the solid red line. Similarly, each spectrum over the temperature range 225–270 K is analyzed. Here we would like to mention that the Gaussian component was included in the fitting procedure to represent the broad band, as this feature appeared distinctly without the sharp peaks below 225 K and reappeared again at 280 K. The peaks $X2$ and $X7$ are observed in all spectra as small kinks over the broad band [see Fig. 3(b)]. $X8$ is the phonon mode ($P1$), which we have discussed earlier. The variation of peak position with the temperature of all these spectral features is shown in Fig. 5(b). The error bars are the standard deviation of the peak positions as obtained from the fitting procedure. It is to be noted that except $X1$, $X2$, $X7$, and $X8$, the rest of the peaks exhibit hardening with the rise in temperature. One expects a decrease in the wave number of a phonon mode with an increase in temperature due to the increase in anharmonicity [45], which indeed we observe for $X1$, $X2$, $X7$, and $X8$. It is to be noted that the peak $X1$ is relatively weak [see Fig. 5(a)] and hence in the Raman spectra, shown in Fig. 3, its intensity may have been masked by the broad band. As mentioned earlier, the previous structural analysis of the same compound did not exhibit any anomaly in lattice parameters or a phase transition beyond 110 K [25,26]. Thus, the origin of the unusual thermal response of the sharp modes is beyond the simple lattice vibration.

Next, we study the sharp peaks $P1$ at ∼690 cm^{-1} (and the peak at 645 cm^{-1} in the doped compound), which could not be indexed with the space group $P31c$ and $P6_3mc$ (Fig. 2). We refrain from assigning them to a two magnon mode, as it appears even at room temperature as compared to the reported $T_N = 110$ K by neutron diffraction [26]. These peaks could not be attributed to a combination mode of observed low wave-number peaks in Fig. 2 either. The sharpness of these peaks prompted us to believe that they do not arise due to flux states of spin excitations of Wigner fermions [46] either. It is likely that the observed peak $P1$ and the one at 645 cm^{-1} are distortion-induced asymmetrical stretching and scissoring vibrational modes involving Co and O ions in CoO_4 tetrahedra containing either the kagome plane or the triangular plane or both in a nonstoichiometric compound [36]. It is to be noted that the intensity of this mode drops in the doped compound, in which the lattice distortion and disorder are less (as revealed by neutron diffraction measurements in Ref. [26]). Here we would like to mention that the cobalites have a unique ability to adsorb and desorb oxygen even at very low temperatures [47]. The complexity in structure arises due to the inhomogeneity of the oxygen content of the samples. Thus, the reported Raman spectral profiles of $YBaCo_4O_{7+\delta}$ differ widely in the literature [36–38], possibly due to the deviation from the pure stoichiometry of this compound, prepared under different conditions.

We discuss below the spectral features of the profile of the sharp peak $P1$ with temperature. Our focus is on the line shape and its temperature dependence, which are highlighted in Fig. 6. All spectra over 660–720 cm^{-1} are fitted with a Fano line shape, $I(\omega) = I_0(q + \varepsilon)^2/(1 + \varepsilon^2)$, $\varepsilon = (\omega - \omega_F)/\Gamma$ after subtraction of a linear background (see Fig. S4 in the Supplemental Material [39]). The temperature dependent Raman shift (ω_F), width (Γ), intensity (I_0), and the Fano asymmetry parameter (q) are shown in Fig. 6. The error bars to the data point for Raman shift, width, and Fano parameter are estimated from the standard deviation of the curve fitting parameters. Overall the Raman wave number for both compounds undergoes a redshift with the increasing temperature. The unusually large change in Raman shift by ∼15 cm^{-1} of $P1$ for the parent compound $YBaCo_4O_{7+\delta}$ over the temperature range 80–300 K is to be noted.

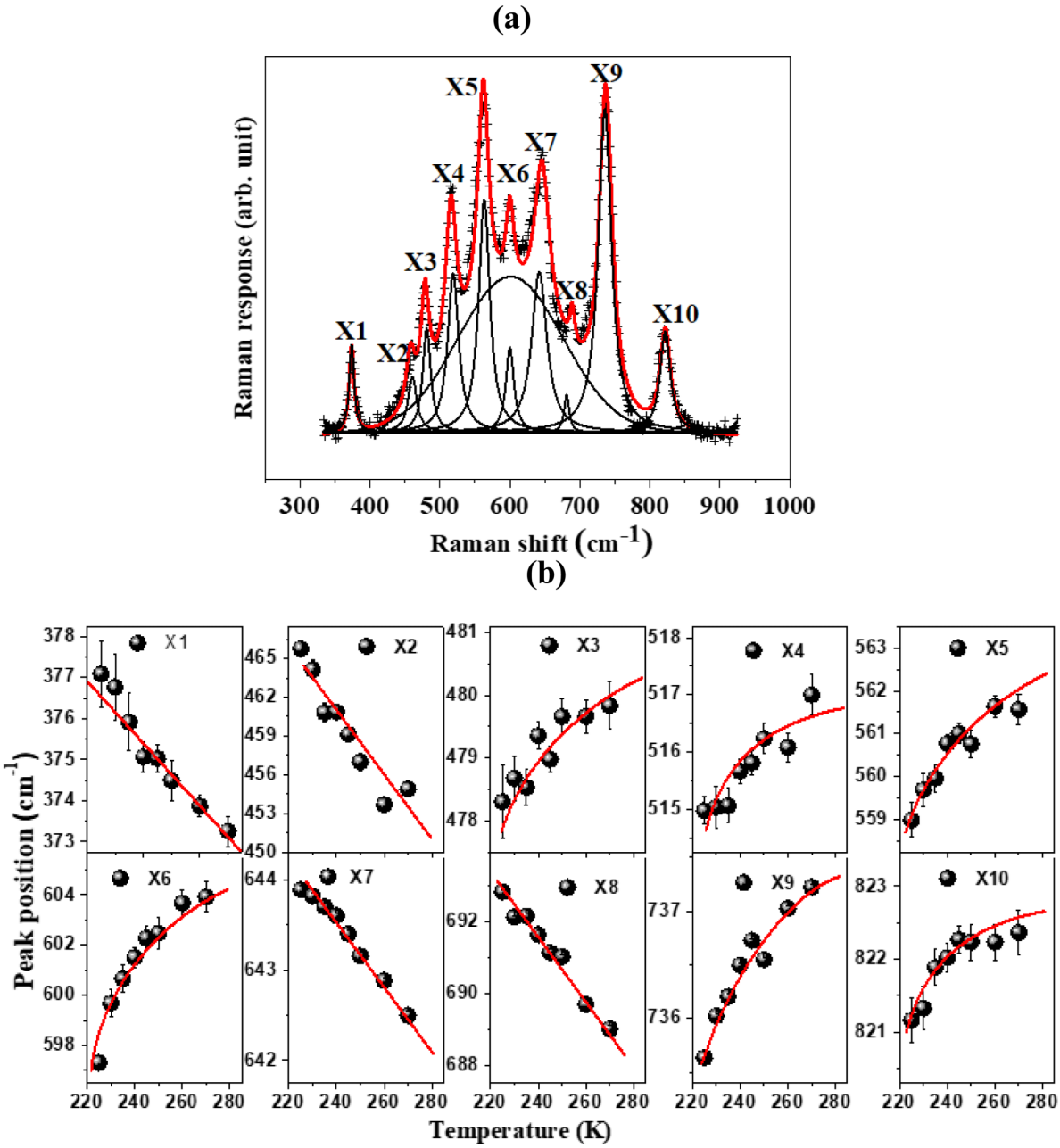

FIG. 5. (a) Raman response in $YBaCo_{3.4}Fe_{0.6}O_7$ at 245 K. The deconvoluted components ($X1$–$X10$) are shown by the black solid lines. The net fitted spectrum is shown by the red solid line. (b) The evolution of the peak positions of $X1$–$X10$ modes with temperature. The error bars are the standard deviation of the peak positions as obtained from the fitting procedure. The solid lines are a guide to the eyes.

Various phenomena can contribute to the shift in the Raman spectral profile with the temperature of a system. We discuss them below in view of their role in explaining the observed behavior of $P1$. By considering the reported thermal expansion of $YBaCo_4O_{7+\delta}$ ~ 0.106 Å^3 over 80–300 K [25] and the Grüneissen parameter $\gamma_j = 2$ (as reported for the related compounds [48]), the expected shift of the $P1$ mode is $\sim 2.18\,\mathrm{cm}^{-1}$ from the relation $\frac{\Delta\omega_j}{\omega_j} = \gamma_j \frac{\Delta V}{V}$, which is much smaller than that observed frequency shift in the present study, $\omega_F \sim 15\,\mathrm{cm}^{-1}$. Therefore, the thermal expansion alone cannot be responsible for the observed shift in the peak position. The shift in phonon frequency and width with the increase in anharmonicity (due to the rise in temperature) can be estimated from the relation $\omega_F(T) = \omega_0 + \Delta(T)$, with $\Delta(T) = A(1 + \frac{2}{e^{\hbar\omega_0/2k_BT}-1})$ and $\Gamma(T) = \Gamma(0)(1 + \frac{2}{e^{\hbar\omega_0/2k_BT}-1})$, respectively. A is the anharmonic constant. ω_0 and $\Gamma(0)$ are Raman shift and width at $T = 0$. The temperature dependence curves of ω_F and Γ over the entire temperature range could not be described by the above equations with physically meaningful values of the ω_0, A, or $\Gamma(0)$. The best fitted curves are shown by the solid lines in Fig. 6(a) with the values of ω_0, A, and Γ_0 as $697.4\,\mathrm{cm}^{-1}$, $-2.7\,\mathrm{cm}^{-1}$, and $10.5\,\mathrm{cm}^{-1}$, respectively, for the parent compound. The same for the doped compound with the values $\omega_0 = 702.2\,\mathrm{cm}^{-1}$,

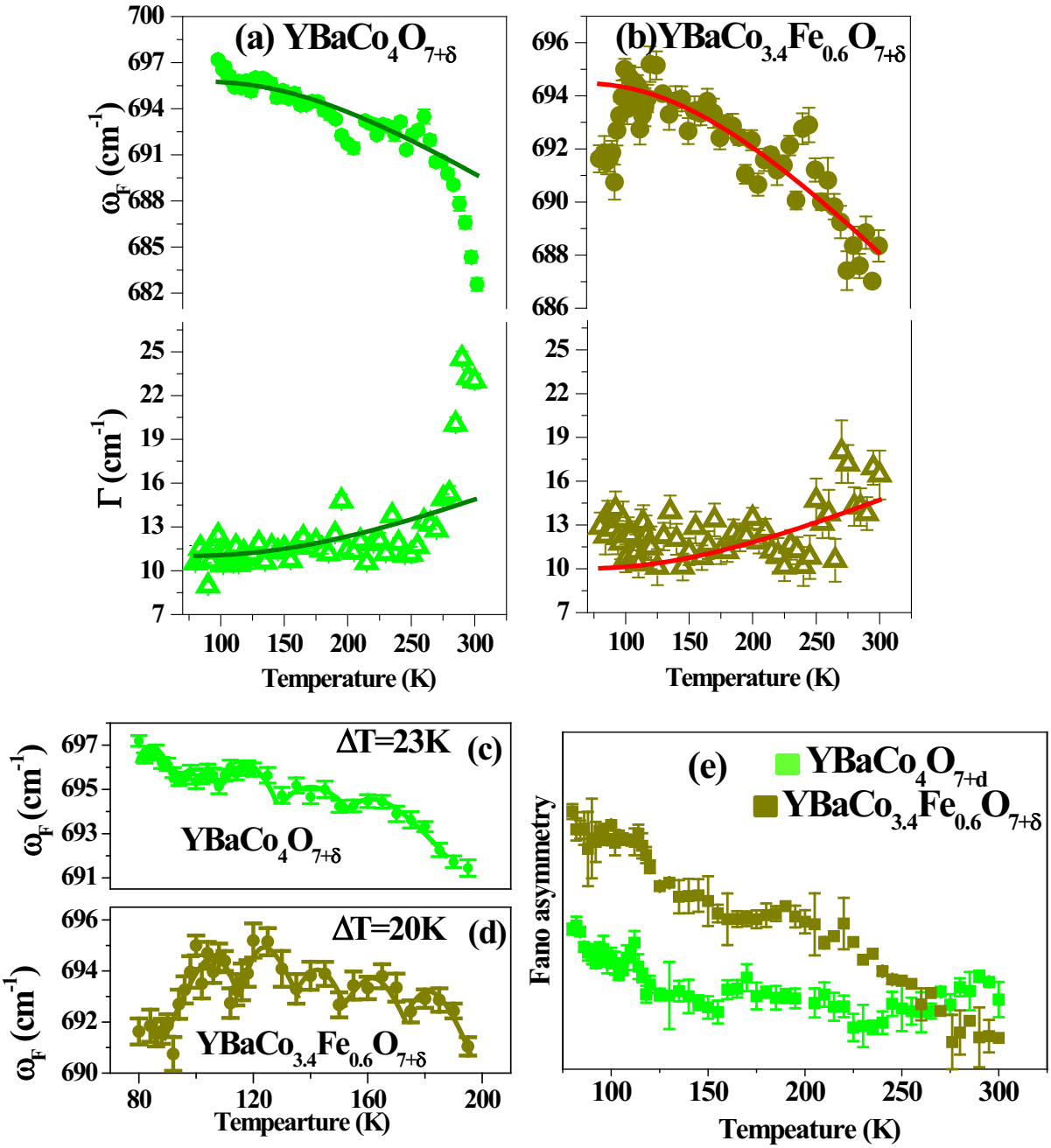

FIG. 6. Variation of ω_F (filled circles) and Γ (open triangles) with temperature for (a) $YBaCo_4O_{7+\delta}$, and $YBaCo_{3.4}Fe_{0.6}O_{7+\delta}$, respectively. The error bar to each data point is the standard deviation of the ω_F as obtained from the fitting procedure. The solid lines are the best fit to the data points as per the equations described in the text. Panels (c) and (d) present the zoomed view of ω_F vs T plot over the temperature range 80–200 K in $YBaCo_4O_{7+\delta}$ and $YBaCo_{3.4}Fe_{0.6}O_{7+\delta}$, respectively. The solid lines are a guide to the eyes. The value of ΔT is the average thermal periodicity of ω_F, as measured between two successive crests and troughs in each panel. (e) The variation of the Fano asymmetry parameter of the peak $P1$ with temperature.

$A = -14.5\,\mathrm{cm}^{-1}$, and $B = 10.2\,\mathrm{cm}^{-1}$, respectively, are shown by the solid lines in Fig. 6(b). The above discussion thus indicates that in addition to the anharmonicity and expansion of the lattice, there are other phenomena that contribute to the Raman scattering for the studied compounds. A careful investigation of the temperature dependence of ω_F reveals that the data points follow an oscillatory nature over the temperature range 80–200 K with a periodicity of ∼23 K, and 20 K for $YBaCo_4O_{7+\delta}$, and $YBaCo_{3.4}Fe_{0.6}O_{7+\delta}$, respectively [Figs. 6(c) and 6(d)]. Though the amplitude of oscillation is within the resolution of our measurements, the reproducibility of the similar oscillatory nature of phonon frequency with temperature for all independent sets of measurements in both compounds is hard to ignore. The modulation in the plot carries the signature of strong coupling between lattice vibration and spin dynamics in the system in an unconventional

way. Furthermore, the increase in Fano asymmetry parameter (q) with decreasing temperature [Fig. 6(e)] indicates that the coupling of the phonon mode with the continuum is enhanced with the lowering of the temperature, especially in the doped $x = 0.6$ compound. The finite value of the asymmetry parameter even at room temperature implies that electron-lattice coupling survives much beyond the antiferromagnetic transition temperature (∼110 K). The observed results indicate a complex interplay between electronic and lattice dynamics, which appears due to a possible synchronization of the crystal structural distortion with the spin-liquid correlations. We refrained from analyzing the Raman peak at 640 cm^{-1}, as it rides over the peak of the broad band and is relatively weak. It was nontrivial to meaningfully analyze this feature over the whole range of temperature under study.

IV. SUMMARY

We report a detailed temperature dependent micro-Raman spectroscopic study on geometrically frustrated layered kagome compounds $YBaCo_{4-x}Fe_xO_{7+\delta}$ ($x = 0$ and 0.6). The broad continuum in the Raman spectra, most likely, illustrates gapped spin liquid phase in this system over the wide measured temperature range 80–300 K. We observe additional sharp spectral features along with the broad band in the high temperature region which show unusual thermal response. The temperature dependent study indicates a strong spin-lattice coupling in these compounds. The present work provokes further theoretical studies to reveal the nature of the spin dynamics of the systems containing alternating triangular-kagome crystal layers having mixed spins and spin/bond disorders. The microscopic mechanism of spin-spin correlation in $YBaCo_{4-x}Fe_xO_{7+\delta}$ with mixed spin structure is expected to be complex and, unfortunately, is still not fully understood.

ACKNOWLEDGMENTS

S.M.Y. and A.R. thank the Board of Research in Nuclear Sciences, Government of India, for financial support. A.R. thanks A. Tarphder in the Department of Physics at IIT Kharagpur for valuable discussion.

[1] L. Savary and L. Balents, Rep. Prog. Phys. **80**, 016502 (2017), and references therein.
[2] J. Knolle and R. Moessner, Annu. Rev. Condens. Matter Phys. **10**, 451 (2019).
[3] X.-G. Wen, Phys. Rev. B **65**, 165113 (2002).
[4] L. Balents, Nature (London) **464**, 199 (2010).
[5] R. Moessner and S. L. Sondhi, Phys. Rev. Lett. **86**, 1881 (2001).
[6] M. Punk, D. Chowdhury, and S. Sachdev, Nat. Phys. **10**, 289 (2014).
[7] A. Kitaev, Ann. Phys. **321**, 2 (2006).
[8] J. Chaloupka, G. Jackeli, and G. Khaliullin, Phys. Rev. Lett. **105**, 027204 (2010).
[9] P. A. McClarty, F. Krüger, T. Guidi, S. F. Parker, and K. Refson, Nat. Phys. **13**, 736 (2017).
[10] S. C. Zhang, T. H. Hansson, and S. Kivelson, Phys. Rev. Lett. **62**, 980(E) (1989).
[11] S. N. Gupta, P. V. Sriluckshmy, K. Mehlawat, A. Balodhi, D. K. Mishra, S. R. Hassan, T. V. Ramakrishnan, D. V. S. Muthu, Y. Singh, and A. K. Sood, Europhys. Lett. **114**, 47004 (2016).
[12] S. N. Gupta, P. V. Sriluckshmy, A. Balodhi, D. V. S. Muthu, S. R. Hassan, Y. Singh, T. V. Ramakrishnan, and A. K. Sood, Phys. Rev. B **94**, 155153 (2016).
[13] A. Glamazda, P. Lemmens, S.-H. Do, Y. S. Choi, and K.-Y. Choi, Nat. Commun. **7**, 12286 (2014).
[14] L. J. Sandilands, Y. Tian, K. W. Plumb, Y.-J. Kim, and K. S. Burch, Phys. Rev. Lett. **114**, 147201 (2015).
[15] J. Nasu, J. Knolle, D. L. Kovrizhin, Y. Motomeand, and R. Moessner, Nat. Phys. **12**, 912 (2016).
[16] J. Y. Lee, Y. Z. You, S. Sachdev, and A. Vishwanath, Phys. Rev. X **9**, 041037 (2019).
[17] Y. J. Uemura, A. Keren, K. Kojima, L. P. Le, G. M. Luke, W. D. Wu, Y. Ajiro, T. Asano, Y. Kuriyama, M. Mekata, H. Kikuchi, and K. Kakurai, Phys. Rev. Lett. **73**, 3306 (1994).
[18] D. Wulferding, P. Lemmens, P. Scheib, J. Röder, P. Mendels, S. Chu, T. Han, and Y. S. Lee, Phys. Rev. B **82**, 144412 (2010).
[19] Y. Qi, C. Xu, and S. Sachdev, Phys. Rev. Lett. **102**, 176401 (2009).
[20] J. A. M. Paddison, M. Daum, Z. Dun, G. Ehlers, Y. Liu, M. B. Stone, H. Zhou, and M. Mourigal, Nat. Phys. **13**, 117 (2017).
[21] B. Perreault, J. Knolle, N. B. Perkins, and F. J. Burnell, Phys. Rev. B **92**, 094439 (2015).
[22] B. Perreault, S. Rachel, F. J. Burnell, and J. Knolle, Phys. Rev. B **95**, 184429 (2017).
[23] W. H. Ko, Z-X. Liu, T-K. Ng, and P. A. Lee, Phys. Rev. B **81**, 024414 (2010).
[24] D. Wulferding, P. Lemmens, H. Yoshida, Y. Okamoto, and Z. Hiroi, J. Phys.: Condens. Matter **24**, 185602 (2012).
[25] A. K. Bera, S. M. Yusuf, and S. Banerjee, Solid State Sci. **16**, 57 (2013).
[26] A. K. Bera, S. M. Yusuf, S. S. Meena, C. Sow, P. S. Anil Kumar, and S. Banerjee, Mater. Res. Express **2**, 026102 (2015).
[27] G. Kresse and D. Joubert, Phys. Rev. B **59**, 1758 (1999)
[28] G. Kresse and J. Furthmüller, Phys. Rev. B **54**, 11169 (1996).
[29] G. Kresse and J. Hafner, Phys. Rev. B **47**, 558 (1993).
[30] J. P. Perdew, K. Burke, and M. Ernzerhof, Phys. Rev. Lett. **77**, 3865 (1996).
[31] M. J. R. Hoch, P. L. Kuhns, S. Yuan, T. Besara, J. B. Whalen, T. Siegrist, A. P. Reyes, J. S. Brooks, H. Zheng, and J. F. Mitchell, Phys. Rev. B **87**, 064419 (2013).
[32] L. C. Chapon, P. G. Radaelli, H. Zheng, and J. F. Mitchell, Phys. Rev. B **74**, 172401 (2006).
[33] M. Soda, Y. Yasui, T. Moyushi, M. Sato, N. Igawa, and K. Kakurai, J. Phys. Soc. Jpn. **75**, 054707 (2006).
[34] P. Manuel, L. C. Chapon, P. G. Radaelli, H. Zheng, and J. F. Mitchell, Phys. Rev. Lett. **103**, 037202 (2009).
[35] S. Lee, W. Lee, K. J. Lee, B. J. Kim, B. J. Suh, H. Zheng, J. F. Mitchell, and K. Y. Choi, Phys. Rev. B **97**, 104409 (2018).
[36] J. L. Izquierdo, J. F. Montoya, A. Gómez, C. Paucar, and O. Morán, Solid State Sci. **12**, 2073 (2010).

[37] R. Nithya, T. G. Kumary, and T. R. Ravindran, AIP Adv. **3**, 022115 (2013).
[38] M. A. Bhat, R. A. Zargar, A. Modi, M. Arora, and N. K. Gaur, Mater. Sci. Poland **34**, 786 (2016).
[39] See Supplemental Material at http://link.aps.org/supplemental/10.1103/PhysRevB.104.144418 for a detailed report on the recorded spectra and the procedures followed to analyze the data.
[40] H. Gretarsson, J. P. Clancy, X. Liu, J. P. Hill, E. Bozin, Y. Singh, S. Manni, P. Gegenwart, J. Kim, A. H. Said, D. Casa, T. Gog, M. H. Upton, H.-S. Kim, J. Yu, V. M. Katukuri, L. Hozoi, J. van den Brink, and Y.-J. Kim, Phys. Rev. Lett. **110**, 076402 (2013).
[41] R. Comin, G. Levy, B. Ludbrook, Z.-H. Zhu, C. N. Veenstra, J. A. Rosen, Y. Singh, P. Gegenwart, D. Stricker, J. N. Hancock, D. van der Marel, I. S. Elfimov, and A. Damascelli, Phys. Rev. Lett. **109**, 266406 (2012).
[42] T.-H. Han, J. S. Helton, S. Chu, D. G. Nocera, J. A. Rodriguez-Rivera, C. Broholm, and Y. S. Lee, Nature (London) **492**, 406 (2012).
[43] J.-W. Mei and X.-G. Wen, arXiv:1507.03007.
[44] D. Wulferding, Y. Choi, W. Lee, and K-Y. Choi, J. Phys.: Condens. Matter **32**, 043001 (2020).
[45] M. Balkanski, R. F. Wallis, and E. Haro, Phys. Rev. B **28**, 1928 (1983).
[46] Y. R. Wang, Phys. Rev. B **46**, 151 (1992).
[47] O. Parkkima and M. Karppinen, Eur. J. Inorg. Chem. **2014**, 4056 (2014).
[48] H. Ledbetter, M. Lei, A. Hermann, and Z. Sheng, Phys. C (Amsterdam, Neth.) **159**, 488 (1989).